Postprint of: Malikan M., Eremeyev V. A.: Post-critical buckling of truncated conical carbon nanotubes considering surface effects embedding in a nonlinear Winkler substrate using the Rayleigh-Ritz method. MATERIALS RESEARCH EXPRESS. (2020). DOI: 10.1088/2053-1591/ab691c

Post-critical buckling of truncated conical carbon nanotubes considering surface effects embedding in a nonlinear Winkler substrate using the Rayleigh-Ritz method

Mohammad Malikan[1]*, Victor A. Eremeyev[1,2]

[1] Department of Mechanics of Materials and Structures, Faculty of Civil and Environmental Engineering, Gdansk University of Technology, 80-233, Gdansk, Poland

[2] Don State Technical University, Gagarina sq., 1, 344000 Rostov on Don, Russia

*Corresponding author

mohammad.malikan@pg.edu.pl, mohammad.malikan@yahoo.com
https://orcid.org/0000-0001-7356-2168

victor.eremeev@pg.edu.pl
https://orcid.org/0000-0002-8128-3262

Abstract

This research predicts theoretically post-critical axial buckling behavior of truncated conical carbon nanotubes (CCNTs) with several boundary conditions by assuming a nonlinear Winkler matrix. The post-buckling of CCNTs has been studied based on the Euler-Bernoulli beam model, Hamilton's principle, Lagrangian strains, and nonlocal

strain gradient theory. Both stiffness-hardening and stiffness-softening properties of the nanostructure are considered by exerting the second stress-gradient and second strain-gradient in the stress and strain fields. Besides small-scale influences, the surface effect is also taken into consideration. The effect of the Winkler foundation is nonlinearly taken into account based on the Taylor expansion. A new admissible function is used in the Rayleigh-Ritz solution technique applicable for buckling and post-buckling of nanotubes and nanobeams. Numerical results and related discussions are compared and reported with those obtained by the literature. The significant results proved that the surface effect and the nonlinear term of the substrate affect the CCNT considerably.

Keywords: Post-critical buckling; Euler-Bernoulli beam; Conical carbon nanotubes; Nonlinear Winkler foundation; Rayleigh-Ritz method

1. Introduction

Carbon nanotubes (CNTs) are hollow ring-shaped structures, comprising carbon atoms. The CNTs can be classified into single- and multi-walled carbon nanotubes (SWCNTs and MWCNTs) and have metallic properties and also quasi-conductivity [1]. These two types of CNTs are already known which are different in the appearance and structure discovered in 1991 and 1993 [2-3], respectively. These types of nanotubes during production can be uncontrollably made in different shapes (twisted, curved, straight, and other irregular geometrical situations). However, another type of irregularity can be made in CNTs, namely nanotubes with a changeable diameter. A CNT with such the inconstant diameter along the length is called conical carbon nanotubes (CCNTs). The CCNTs, due

to dominant applications in the modern industries, have been of important interest to engineers and scientific researchers [4-10]. In the case of CCNTs, Chang and Lee [11] mechanically studied a CCNT in vibrating based on the surface effect. Two boundary conditions, namely, clamped-free and clamped-clamped boundary conditions were applied using the Rayleigh-Ritz method. Lee and Chang [12] analyzed the surface effect for nanotubes and nanowires in vibration. The unique properties of carbon nanotubes, including the high modulus of elasticity and good tensile strength on one side and the carbon nature of CNTs on another side, have led to significant research over the last decade into the efficiency and growth processes of nanotubes' proliferation. Because of difficult conditions and high costs of experiments in nanoscale for considering mechanical behavior of size-dependent nanomaterials, the theoretical researches based on the continuum stress/strain gradients and molecular dynamics simulation have attracted much attention to researchers. Heretofore, in terms of critical stability of straight CNTs, in a molecular mechanics study, Chang et al. [13] studied buckling of CNTs subjected to axial compression. Their important results displayed that the stability of a zigzag CNT is further than an armchair one. Yan et al. [14] modeled the carbon nanotubes as a three-walled shell and analyzed it with exposing to the axial compression forces. They implemented the small-scale influence through the nonlocal elasticity approach. On the other side, the influences of the thermal surround on the buckling loads have been taken. Their achieved mathematical relations were analytically solved based on pivot boundaries. Shima [15] analyzed the nonlinear static buckling of CNTs. Wang et al. [16] developed gradients of stress and strain to investigate the stability of nanoscale tubes by

considering a polymer matrix based on the pivot-pivot Timoshenko beam model. Berrabah et al. [17] investigated axial buckling of hinged nanotubes rested in a polymer medium based on the Timoshenko beam theory. To consider small-scale effects, the nonlocal continuum mechanic was used in the form of Eringen's nonlocal elasticity theory. Akgöz and Civalek [18] considered the Pasternak substrate for an axially compressed hinged-hinged CNT based on the nonlocal elasticity theory. A comprehensive review of the concept of vibration, buckling and thermal analyses of SWCNTs was presented by Rafiee and Moghadam [19]. Different approaches as continuum elasticity, nonlocal elasticity, and molecular dynamics simulation were taken into the investigation. Sudak [20] analyzed axial buckling of concentric multi-walled carbon nanotubes based on the van der Waals forces and using nonlocal elasticity theory. Rahmanian et al. [21] modeled nonlocal elasticity for analysis of fundamental frequencies of CNTs rested on the Winkler medium. They modeled the nanotube into two categories, a beam model and shell one.

Moreover, in terms of post-critical buckling studies, rarely investigations have been done on nanobeams/tubes. Mao and Ling [22] analyzed the post-stability response of thin-walled anisotropic composite beams based on the Fourier expansion. The nonlinear equations were solved using the Galerkin procedure. Song and Li [23] modeled a pinned-fixed classical local beam subjected to the thermal environment under thermal stability and post-stability situations. The beam was also placed on a polymer foundation. Challamel [24] investigated elastic beams under post-buckling conditions and assumed a gradient foundation by using an exact solution method. Silvestre et al. [25] presented a

molecular dynamics simulation to study buckling and post-buckling of CNTs under pure twisting. Ansari et al. [26] predicted post- thermomechanical buckling response of nonlocal Euler-Bernoulli SWCNTs by considering thermal and axial in-plane forces. Akbas [27] studied post-critical stability with a large behavior for axially compressed the Timoshenko beam model. Ansari et al. [28] employed nonlocal elasticity theory to examine size-dependent effects for a Timoshenko SWCNT under buckling and post-buckling conditions. Recently, She et al. [29] developed functionality and porosity for a SWCNT under thermal stability and post-buckling condition. They applied both stress nonlocality and microstructural size dependency to evaluate the nanotube in a nanoscale schema. The obtained nonlinear equations were solved based on the two-step perturbation technique. Dai et al. [30] assumed an axial magnetic field around nanotubes and derived exact modes to analyze nonlocal post-buckling of CNTs.

The review of the above research related to static buckling and post-buckling of CNTs vividly showed that there is no paper in which a truncated CCNT is studied under post-buckling conditions. This led to the motivation of authors to write this paper. This research also considers both stiffness-hardening and stiffness-softening and also nonlinear behavior of Winkler foundation. To this, the Euler-Bernoulli beam model is applied in the energy method via Hamilton's principle by employing nonlinear Lagrangian strains. To examine small-scale effects, nonlocal strain gradient theory is taken into consideration which includes microstructural size-dependent effects and a second stress gradient. In light of the importance of the surface effect for nanomaterials, the effect is here investigated. The Winkler matrix covers the tube and behaviors

nonlinearly based on the Taylor expansion. To solve the post-buckling mathematical relations, the Rayleigh-Ritz solution method is applied based on a new shape function. By using this function, the post-critical buckling load can be presented for several boundary conditions particularly free edges. Thereafter, numerical results are shown by changes in the essential and key parameters with and without considering the nonlinear behavior of the foundation.

2. The constitutive model

2.1 Energy formulation

Fig. 1 in a Cartesian coordinate system displays a CCNT. The symbols are respectively, the thickness of the tube (h), the exterior radius of the smaller diameter of the tube (R_{1o}), the internal radius of the smaller diameter of the tube (R_{1i}), the inner radius of the larger diameter of the tube (R_{2o}), and the taper angle (θ).

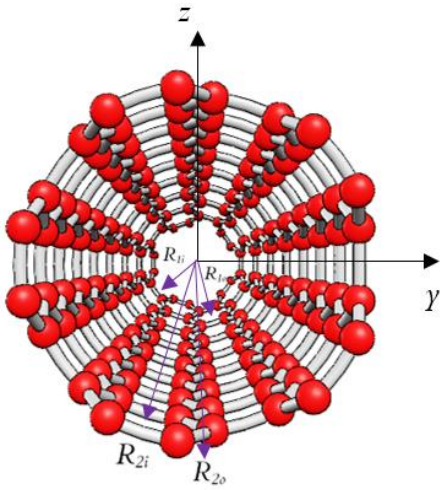

(a)

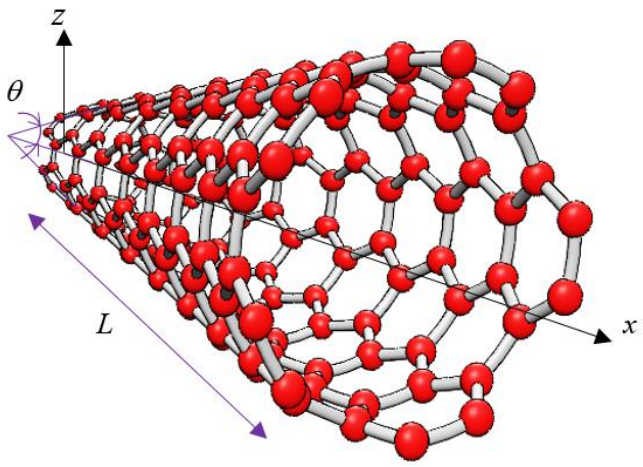

(b)

Fig. 1. Cross section (a) and three-dimensional (b) of the CCNT

To assume the motion of nanotubes' nodes, the classical beam theory is applied [23]. According to this beam approach the displacement field can be expanded as

$$\begin{Bmatrix} u_1(x,z) \\ u_3(x,z) \end{Bmatrix} = \begin{Bmatrix} u(x) - z\,\dfrac{dw(x)}{dx} \\ w(x) \end{Bmatrix} \tag{1a-b}$$

in which $u_1(x,z)$ and $u_3(x,z)$ represent the displacement of points along x and z-axis and $u(x)$ and $w(x)$ are displacement of the mid-surface of the undeformed CCNT along x and z-axis. Moreover, z is a coordinate for the thickness direction in the continuum domain. First, the Hamilton principle is defined as

$$\delta\Pi = \int_{t_1}^{t_2} (\delta W - \delta U)\, dt = 0 \tag{2}$$

in which δU, and δW are virtual strain energy and work done by external forces, respectively.

The virtual strain energy and the work done by external forces would be formulated as

$$U = \frac{1}{2}\int_0^L \int_A \sigma_{xx}\varepsilon_{xx} dA dx \rightarrow \delta U = \int_0^L \int_A \sigma_{xx}\delta\varepsilon_{xx} dA dx \tag{3}$$

$$W = -\frac{1}{2}\int_0^L \left[N_x \left(\frac{dw}{dx}\right)^2 + K_W w \right] dx \rightarrow \delta W = -\int_0^L \left(N^0 \frac{dw}{dx}\frac{d\,\delta w}{dx} + K_W\,\delta w \right) dx \tag{4}$$

in which δU (Note that δ means the variations of the energies) shows the virtual strain energy, σ and ε are the stress and strain tensors and also dV displays the integral on the volume of the domain. Furthermore, K_W is the Winkler foundation. It is assumed that the post-buckling axial force is as N_x =- N^0 where N^0 demonstrates the post-critical axial buckling load (PCL).

The tensor of nonlinear strains can be obtained based on the applying nonlinear Lagrangian strains on Eqs. (1) which leads to

$$\{\varepsilon_{xx}\} = \left\{ \frac{du}{dx} - z\,\frac{d^2w}{dx^2} + \frac{1}{2}\left(\frac{dw}{dx}\right)^2 \right\} \tag{5}$$

The local stress resultants can be written as

$$\begin{Bmatrix} N_x \\ M_x \end{Bmatrix} = \int_A \begin{Bmatrix} \sigma_x \\ \sigma_x z \end{Bmatrix} dA \tag{6a-b}$$

in which the in-plane, moment and shear stress resultants are N_x, M_x and Q_x, respectively. Therefore, based on the Eq. (5), Eqs. (6) can be expanded as

$$\begin{Bmatrix} N_x \\ M_x \end{Bmatrix} = \begin{Bmatrix} E_e A_e \left[\dfrac{du}{dx} + \dfrac{1}{2}\left(\dfrac{dw}{dx}\right)^2 \right] \\ E_e I_c \dfrac{d^2w}{dx^2} \end{Bmatrix} \tag{7a-b}$$

in which $I_c = \dfrac{\pi\left(R_o^4 - R_i^4\right)}{4}$ represents the moment of area of the cross section.

Meanwhile, the relationship between the equivalent smaller and larger radii of the CCNT can be derived as

$$R_o = R_{1o} + x\,\sin(\theta) \tag{8a}$$

$$R_i = R_{1i} + x\,\sin(\theta) \tag{8b}$$

where R_o and R_i denote equivalent inner and outer radii for a straight CNT which resulted from the conic CNT. For the large elasticity domains, the surface effect can be ignorable. However, for a small-scale particle, the effect of the surface becomes important due to the high surface-to-volume ratio [11-12]. To study such an effect, the following relation can be employed [11]

$$E_e A_e = EA + E_s A_s = \pi E\left(R_o^2 - R_i^2\right) + 2\pi E_s\left(R_o^2 + R_i^2\right) \tag{9}$$

in which *Es* and *As* depict surface elasticity and surface area modules, *E* denotes the Young's modulus and *A* is the cross section area of the nanotube.

Assigning $\delta\Pi=0$, the constitutive equation would be derived for a CCNT as

$$\delta u = 0 \;:\frac{dN_x}{dx} = 0 \tag{10a}$$

$$\delta w = 0 \;:\frac{d^2 M_x}{dx^2} - N^0\frac{d^2 w}{dx^2} - K_W = 0 \tag{10b}$$

The nonlinear Winkler model (Fig. 2) can be estimated by the third-order term of Taylor expansion as [31-32]

$$K_W = k_{w-L} w + k_{w-NL} w^3 \tag{11}$$

in which k_{w-L} and k_{w-NL} are symbolized to show linear and nonlinear values of the foundation module.

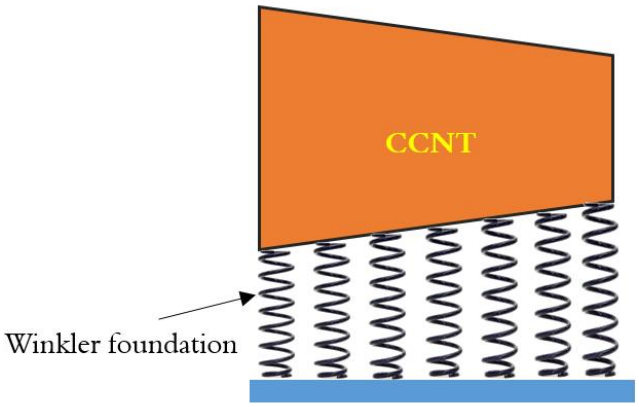

Fig. 2. The Winkler model covers the CCNT

2.2 The size-dependent effects

To take into consideration the stress nonlocality and microstructural size-dependent effects, the nonlocal strain gradient theory (NSGT) is given by [33]

$$\left(1-\mu\frac{d^2}{dx^2}\right)\sigma_{xx}=C_{ijkl}\left(1-l^2\frac{d^2}{dx^2}\right)\varepsilon_{xx} \tag{12}$$

in which μ depicts nonlocality which is equal to $(e_0a)^2$ and also l denotes a length scale factor in the NSGT. Moreover, e shows a physical constant and a=0.142 nm is the bond length of carbon-carbon atoms.

By substituting Eq. (12) into Eqs. (7), the small-scale stress resultants can be obtained as [34-48]

$$N_x-\mu\frac{d^2N_x}{dx^2}=E_eA_e\left(1-l^2\frac{d^2}{dx^2}\right)\left\{\frac{du}{dx}+\frac{1}{2}\left(\frac{dw}{dx}\right)^2\right\} \tag{13}$$

$$M_x - \mu \frac{d^2 M_x}{dx^2} = -E_e I_c \left(1 - l^2 \frac{d^2}{dx^2}\right)\left\{\frac{d^2 w}{dx^2}\right\} \tag{14}$$

And from Eqs. (7a), (10a) and (13), the axial stress resultant in a nonlocal strain gradient form can be expressed as

$$N_x = \mu \frac{d}{dx}\left(\frac{dN_x}{dx}\right) + E_e A_e \left(1 - l^2 \frac{d^2}{dx^2}\right)\left\{\frac{du}{dx} + \frac{1}{2}\left(\frac{dw}{dx}\right)^2\right\};\ \left\{\frac{dN_x}{dx} = 0\right\} \tag{15}$$

As the initial axial displacements for beams with immovable ends should be set to zero, hence

$$u\left(x = 0\right) = 0;\quad u\left(x = L\right) = 0 \tag{16}$$

Then

$$N_x = E_e A_e \left(1 - l^2 \frac{d^2}{dx^2}\right)\left\{\frac{1}{2}\left(\frac{dw}{dx}\right)^2\right\} \tag{17}$$

And from Eqs. (7b), (10b) and (14), the bending moment stress resultant in a nonlocal strain gradient form can be expressed as

$$M_x = -E_e I_c \left(1 - l^2 \frac{d^2}{dx^2}\right)\left\{\frac{d^2 w}{dx^2}\right\} + \mu\left(N^0 \frac{d^2 w}{dx^2} + K_W\right) \tag{18}$$

Then, the strain energy can be written as below

$$U = \int_0^L \int_A \sigma_{xx} \varepsilon_{xx} dA dx = \int_0^L \int_A \sigma_{xx} \left\{-z \frac{d^2 w}{dx^2} + \frac{1}{2}\left(\frac{dw}{dx}\right)^2\right\} dA dx \Rightarrow$$

$$U = \int_0^L \left(-M_x \frac{d^2 w}{dx^2} + \frac{1}{2} N_x \left(\frac{dw}{dx}\right)^2\right) dx \Rightarrow$$

$$U=\int_0^L\left\{-\left[-E_eI_c\left(1-l^2\frac{d^2}{dx^2}\right)\left(\frac{d^2w}{dx^2}\right)^2+\mu\left(N^0\left(\frac{d^2w}{dx^2}\right)^2+K_W\frac{d^2w}{dx^2}\right)\right]\right.$$
$$\left.-E_eA_e\left(1-l^2\frac{d^2}{dx^2}\right)\left[\frac{1}{4}\left(\frac{dw}{dx}\right)^4\right]\right\}dx \tag{19}$$

Therefore, the equation of post-critical buckling load can be achieved as

$$U+W=\int_0^L\left\{\left[E_eI_c\left(1-l^2\frac{d^2}{dx^2}\right)\left(\frac{d^2w}{dx^2}\right)^2-\mu\left(N^0\left(\frac{d^2w}{dx^2}\right)^2+K_W\frac{d^2w}{dx^2}\right)\right]\right.$$
$$\left.-E_eA_e\left(1-l^2\frac{d^2}{dx^2}\right)\left[\frac{1}{4}\left(\frac{dw}{dx}\right)^4\right]+\left[N^0\left(\frac{dw}{dx}\right)^2+K_Ww\right]\right\}dx=0 \tag{20}$$

Consequently, the aforementioned post-buckling relations for a CCNT with assuming nonlinear behavior of the matrix will be

$$\int_0^L\left[E_eI_c\left(1-l^2\frac{d^2}{dx^2}\right)\left(\frac{d^2w}{dx^2}\right)^2\right]dx-N^0\int_0^L\left[\left(\frac{dw}{dx}\right)^2+\mu\left(\frac{d^2w}{dx^2}\right)^2\right]dx$$
$$+\int_0^L\left(K_{w-L}w+K_{w-NL}w^3\right)\left(1-\mu\frac{d^2w}{dx^2}\right)dx \tag{21}$$
$$-\int_0^L\left\{E_eA_e\left(1-l^2\frac{d^2}{dx^2}\right)\left[\frac{1}{4}\left(\frac{dw}{dx}\right)^4\right]\right\}dx=0$$

3. Rayleigh-Ritz solution process

As the post-buckling discussions are geometrically nonlinear ones; therefore, in order to solve nonlinear eigenvalue problems, the Rayleigh-Ritz solution technique can be a good choice [49-52], owing to its capability to give high accurate numerical outcomes. The method is a semi-analytical one and satisfies eigenvalue problems, a few of which should be solved nonlinearly for which the numerical solutions have to be employed. However,

such numerical methods have larger solution time [53-56] and cannot be cost-effective. Hence, semi-analytical methods can be a better suggestion to solve nonlinear eigenvalue problems, for example, post-buckling ones. The transverse displacement for the Rayleigh-Ritz method was presented as [52]

$$w\left(x,t\right)=\sum_{i=1}^{N}a_i\varphi_i\left(x,t\right)\exp\left(\omega t\sqrt{-1}\right) \tag{22}$$

in which $\varphi_i\left(x,t\right)$ is the fundamental mode shapes and ω is the natural frequency in vibration analyses based on time. Further, a_i represents the unknown variable which should be calculated for deflection analyses.

$$\varphi_i\left(x,t\right)=f_\varphi T_i\left(x,t\right)=f_\varphi x^{i-1} \tag{23}$$

The only difficult thing in the semi-analytical solution methods like the Rayleigh-Ritz might be determining mode shapes which should satisfy boundary conditions. In this research, a new mode shape is assumed by which a very good agreement has been obtained while comparing the numerical outcomes with the literature [49-52]. The mode shape which determines several boundary conditions is innovatively derived as below

$$f_\varphi=\left(\frac{x}{L}\right)^{\eta}\times\left(1-\frac{x}{L}\right)^{\zeta} \tag{24}$$

in which η and ζ define several boundary conditions as shown by Table 1.

Table 1. Admissible quantities for several boundary conditions

Boundary conditions	$\eta(x=0)$	$\zeta(x=L)$
SS	1	1
SC	1	2
CS	2	1
CC	2	2
CF	2	0
FC	0	2

The conditions alluded in Table 1 can satisfy the geometrical and force boundary conditions given in Table 2. The stress resultants in boundaries can be written in the nonlocal strain gradient forms as force boundary conditions [57]. There are also other references in which the nonlocal boundary conditions are presented [58-60].

Table 2. Essential and Natural boundary conditions

Configurations	In nonlocal strain gradient conditions at $(0, L)$	In local conditions ($l = \mu = 0$) at $(0, L)$
S	$w=0$ $M = 0$ $M_h = 0$	$w=0$ $M_{cl} = 0$
C	$w=0$ $w'=0$ $M \neq 0$ $M_h \neq 0$	$w=0$ $w'=0$ $M_{cl} \neq 0$
F	$w\neq 0$ $N = \left(1 - l^2 \frac{d^2}{dx^2}\right) N_{cl} = 0$ $M = -\left(1 + l^2 \frac{d^2}{dx^2}\right) M_{cl} + \mu \frac{d}{dx}\left(N_{cl} \frac{dw}{dx}\right) = 0$ $Q = \left(1 - l^2 \frac{d^2}{dx^2}\right) \frac{dM_{cl}}{dx} + \left(1 - \mu \frac{d^2}{dx^2}\right)\left(N_{cl} \frac{dw}{dx}\right) = 0$ $N_h = N_{cl} = 0$ $M_h = \frac{dM_{cl}}{dx} = 0$	$w\neq 0$ $N = N_{cl} = 0$ $M = M_{cl} = 0$ $Q = Q_{cl} = 0$

* *cl* and *h* in sub-indexes mean classical and higher-order cases, respectively.

4. Accuracy of results

To use the semi-analytical polynomial methods like the Rayleigh-Ritz one, first, the convergence rate of the solution method should be investigated. To this, Fig. 3 is presented with which it is observed that a suitable rate for convergence of the solution can be chosen as N=5. By choosing the value, the numerical outcomes would be acquired correctly. Moreover, due to solving a symmetrical problem and being the beam an isotropic one, naturally, the behavior of the SC should be as same as the CS boundary conditions. Note that this claim can be true for CF and FC boundaries.

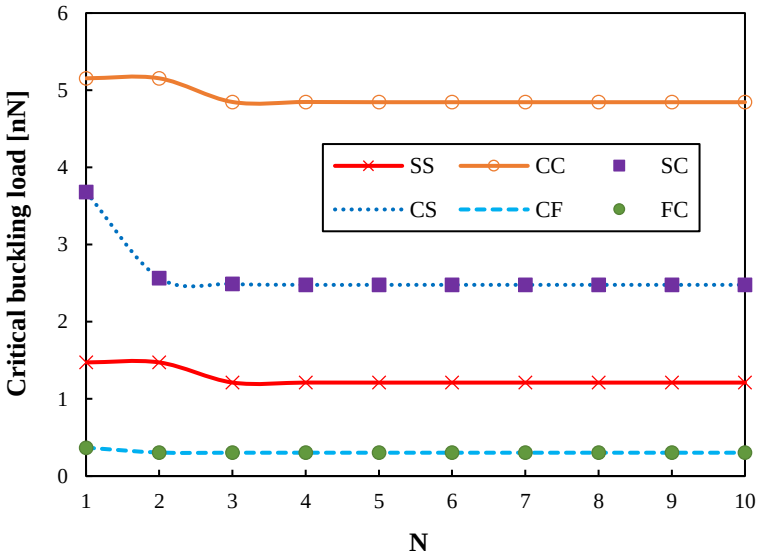

Fig. 3. The convergence rate of the Rayleigh-Ritz vs. different boundary conditions for a SWCNT ($l=0$, $e_0a=0$, $L=20d$, $E=1TPa$, $v=0.19$, $d=1nm$)

The numerical results and the related discussion would be begun with the formulation's validation. To do this, according to Tables 3-6 taken from references [61-62], the critical buckling load of a nanobeam is evaluated whilst the elasticity properties were chosen as $E=1TPa$, $\upsilon= 0.19$, and diameter of the beam was selected as $d=1nm$. The numerical

results within the Tables are for the Euler-Bernoulli beam equation solved with an explicit analytical solution [61] and the differential transform method (DTM) [62]. As it is found, in the three cases ($\mu=0\ nm^2$, $\mu=1\ nm^2$, *and* $\mu=2\ nm^2$), the results of the references and the present work are close to each other and reveal an excellent agreement into clamped-clamped, hinged-hinged and clamped-free boundary conditions. Although the results of clamped-hinged boundary conditions are slightly farther from the literature, it can be acceptable. These Tables approve the efficiency and accuracy of the present admissible function for various boundary conditions.

Table 3. Comparison of critical loads originated from literature for a hinged-hinged beam.

	P_{Cr} *(nN)*								
	$\mu=0\ nm^2$			$\mu=1\ nm^2$			$\mu=4\ nm^2$		
L (nm)	[61], EB, Explicit	[62], EB, DTM	Present-EB, Rayleigh-Ritz	[61]	[62]	Present	[61]	[62]	Present
10	4.8447	4.8447	4.8447	4.4095	4.4095	4.4095	3.4735	3.4735	3.4735
12	3.3644	3.3644	3.3644	3.1486	3.1486	3.1486	2.6405	2.6405	2.6405
14	2.4718	2.4718	2.4718	2.3533	2.3533	2.3533	2.0574	2.0574	2.0574
16	1.8925	1.8925	1.8925	1.8222	1.8222	1.8222	1.6396	1.6396	1.6396
18	1.4953	1.4953	1.4953	1.4511	1.4511	1.4511	1.3329	1.3329	1.3329
20	1.2112	1.2112	1.2112	1.182	1.182	1.182	1.1024	1.1024	1.1024

Table 4. Comparison of critical loads originated from literature for a clamped-hinged beam.

	P_{Cr} (nN)								
	$\mu=0$ nm^2			$\mu=1$ nm^2			$\mu=2$ nm^2		
L (nm)	[61], EB, Explicit	[62], EB, DTM	Present-EB, Rayleigh-Ritz	[61]	[62]	Present	[61]	[62]	Present
10	9.887	9.887	9.911	8.2295	8.2295	8.2461	7.048	7.048	7.060
12	6.886	6.886	6.883	6.0235	6.0235	6.0363	5.3651	5.3651	5.3753
14	5.044	5.044	5.056	4.5744	4.5744	4.5844	4.1844	4.1844	4.1928
16	3.8621	3.8621	3.8715	3.5804	3.5804	3.5884	3.337	3.337	3.344
18	3.0516	3.0516	3.0589	2.873	2.873	2.879	2.7141	2.7141	2.7199
20	2.4718	2.4718	2.4777	2.3533	2.3533	2.3587	2.2456	2.2456	2.2505

Table 5. Comparison of critical loads originated from literature for a clamped-clamped beam.

	P_{Cr} (nN)								
	$\mu=0$ nm^2			$\mu=1$ nm^2			$\mu=2$ nm^2		
L (nm)	[61], EB, Explicit	[62], EB, DTM	Present-EB, Rayleigh-Ritz	[61]	[62]	Present	[61]	[62]	Present
10	19.379	19.379	19.379	13.8939	13.8939	13.8938	10.828	10.828	10.828
12	13.458	13.458	13.458	10.652	10.652	10.652	8.6917	8.6917	8.6917
14	9.877	9.877	9.887	8.2296	8.2296	8.2296	7.0479	7.0479	7.0479
16	7.4699	7.4699	7.4699	6.5585	6.5585	6.5585	5.7854	5.7854	5.7855
18	5.9811	5.9811	5.9811	5.3375	5.3375	5.3375	4.8091	4.8091	4.8091
20	4.8447	4.8447	4.8447	4.4095	4.4095	4.4095	4.046	4.046	4.046

Table 6. Comparison of critical loads originated from literature for a clamped-free beam.

	P_{Cr} (nN)								
	$\mu=0\ nm^2$			$\mu=1\ nm^2$			$\mu=2\ nm^2$		
L (nm)	[61], EB, Explicit	[62], EB, DTM	Present-EB, Rayleigh-Ritz	[61]	[62]	Present	[61]	[62]	Present
10	1.2112	1.2112	1.2112	1.1820	1.1820	1.1820	1.1542	1.1542	1.1542
12	0.8411	0.8411	0.8411	0.8269	0.8269	0.8269	0.8132	0.8132	0.8132
14	0.6179	0.6179	0.6179	0.6103	0.6103	0.6103	0.6027	0.6027	0.6027
16	0.4731	0.4731	0.4731	0.4686	0.4686	0.4686	0.4641	0.4641	0.4641
18	0.3738	0.3738	0.3738	0.3710	0.3710	0.3710	0.3682	0.3682	0.3682
20	0.3028	0.3028	0.3028	0.3009	0.3009	0.3009	0.2991	0.2991	0.2991

In addition to the above validation of the present solution's shape function, we can use the ref. [63] in which some admissible functions were employed (Table 7) which had appropriate results. As can be noticed, Fig. 4 exhibits an excellent agreement between the results of the present admissible function with those obtained from ref. [63]. The superiority of the present admissible function versus those pointed out in Table 7 can be the possibility of applying free edges and also simpler utilization and application.

Table 7. Admissible functions from literature

Boundary conditions	Suitable functions
SS	$Sin(\pi x/L)$
CC	$0.5(1-Cos(2\pi x/L)$ or $Sin^2(\pi x/L)$
CS	$0.1709382933(\mathrm{Sin}(k_1 x)- k_1 L Cos(k_1 x)+ k_1 L(1-(x/L)))$ $k_1=1.4318\pi/L$

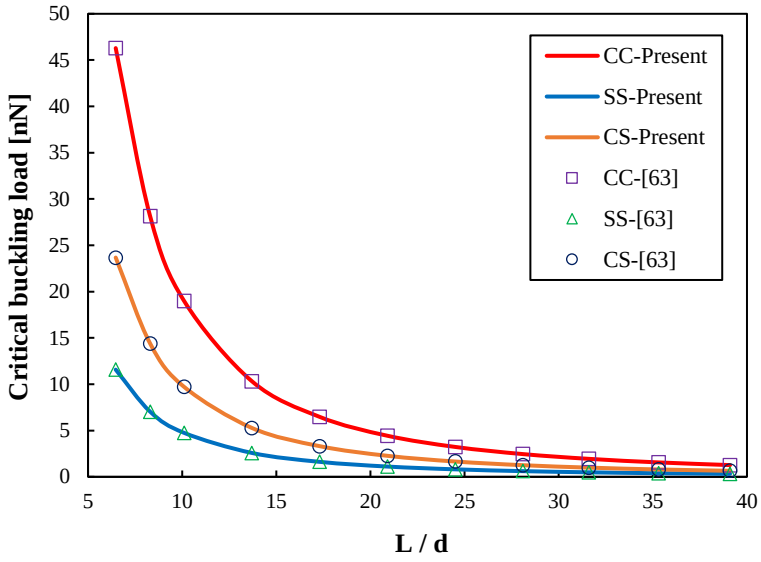

Fig. 4. Comparison of critical buckling loads for several boundary conditions vs. literature for a SWCNT ($l=0$, $e_0a=0$, $E=1TPa$, $v=0.19$, $d=1nm$)

5. Post-buckling of truncated conical SWCNTs

This section is concerned to assess and predict the post-critical buckling loads (PCL) of a truncated conical carbon nanotube (CCNT). First, in order to analyze the CCNT, the following material properties are utilized as [63-72]

0.5 nm$<e_0a<$0.8 nm [64], 0$<e_0a\leq$2 nm [65-66],
E=1000 nN/nm^2, v=0.19, Es=5.1882 N/m
h=0.066 nm, R_{1o}=0.5 nm, d=2 R_{1o}

It is important to note that the above-mentioned quantities are averaged values and are related to an armchair carbon nanotube in a continuum schema [73-78]. As the armchair is a symmetrical nanotube, it is presumed as an isotropic beam.

To describe the influences of the Winkler foundation, Fig. 5a is shown for which the CCNT is in two cases, with the foundation and without it. To do this, SS boundary

conditions are taken into consideration. It is simply seen that increasing the length-to-diameter ratio whilst the foundation is eliminated leads to dropping the slope of the results of the PCL. However, while the foundation is embedded, the slope of the results decreased so that L/d=15 and then the slope goes up rapidly. These contrary outcomes for both cases can be interpreted physically based on the reverse transverse forces of the foundation. This means that when the CCNT is larger, the matrix embraces a stronger foundation. Because the foundation depends on the length of the model. And its length increases with the increase of the length of the CCNT, which leads to further stiffness of the medium.

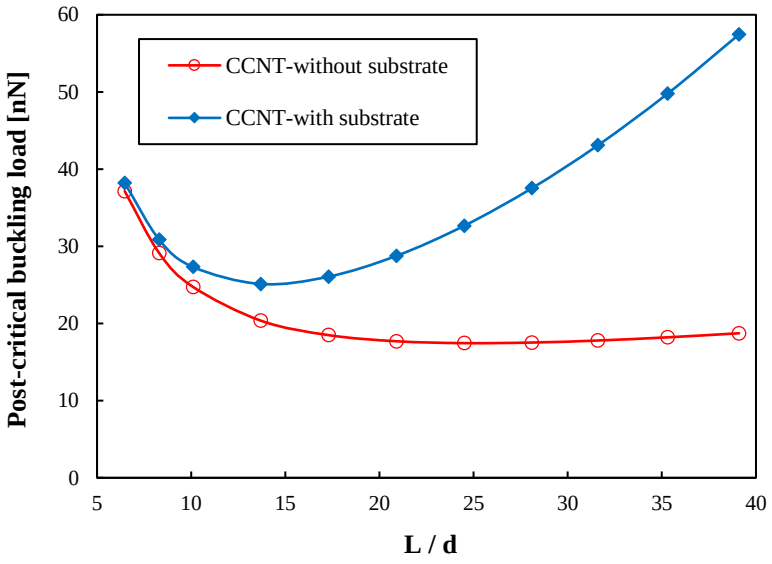

Fig. 5a. Post-critical buckling loads for present and absent of the foundation ($\theta=\pi/36$, $k_{w\text{-}L}=0.1GPa$, $k_{w\text{-}NL}=0.2GPa$, $e_0a=0.5$ *nm*, $l=0.1$ *nm*, *SS*)

On the other hand, Fig. 5b briefly examines several small-scale models for the CCNT with the increase of the length-to-diameter ratio for SS boundary conditions. There are strain gradient theory (SGT) for which we take e_0a=0 and l=0.5 nm, nonlocal theory of Eringen (NT) for which we have e_0a=0.5 nm and l=0, nonlocal strain gradient theory

(NSGT) for which the e_0a=0 and l=0.2 nm are used and classical (local) mechanics for which the e_0a=0 and l=0 should be employed. As it is clear, the large CCNTs make the various size-dependent theories insignificant leading to a macro scale model. In the nanoscale model, the SGT, separately, cannot be applicable in light of its results which are greater than classical mechanics. But, the NT and NSGT pose closer results to each other, and these are more executive theories in terms of continuum mechanics of nanomaterials. It is worth mentioning that the NSGT strongly depends on the value of the length scale parameter which can be determined for each nanomaterial in an experiment.

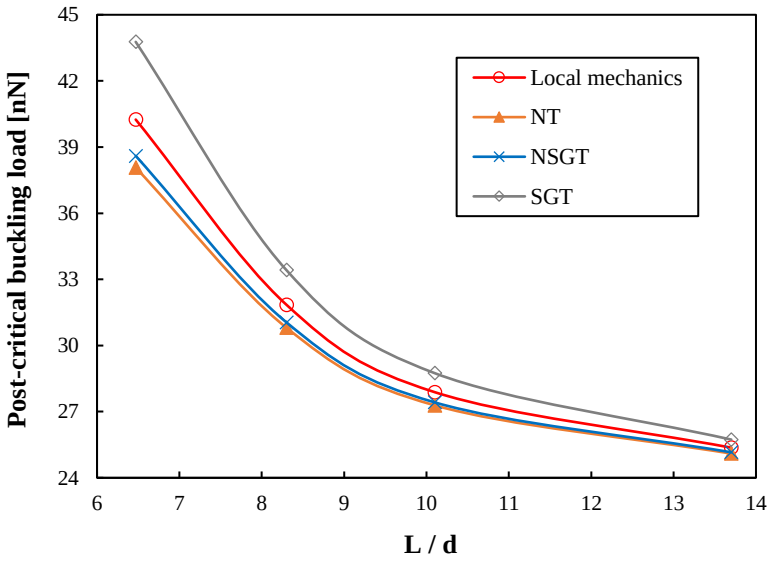

Fig. 5b. Post-critical buckling loads for several small-scale theories ($\theta=\pi/36$, $k_{w\text{-}L}=0.1GPa$, $k_{w\text{-}NL}=0.2GPa$, *SS*)

Fig. 6a considers the effects of the nonlinear term of the substrate versus the linear one by shifts in the strain gradient length scale parameter. As the literature proved it [79], in order to show the microstructural size-dependency of the nanostructures, there is a need to use the length scale parameter. The increase in this parameter presents a larger stiffness

of the nanomaterial. Such the property which is owing to lessening of size of the material from the macro up to nano has been found in the experiments for some micro/nanomaterials [80-82]. It is noteworthy to state that the influence of the nonlinear term is smaller than the linear one on the PCL. This is because the numerical results for post-buckling by use of the linear term of the Winkler are greater values in contrast to the results of the nonlinear term of the foundation. This result is taken from the four cases of Fig. 6a.

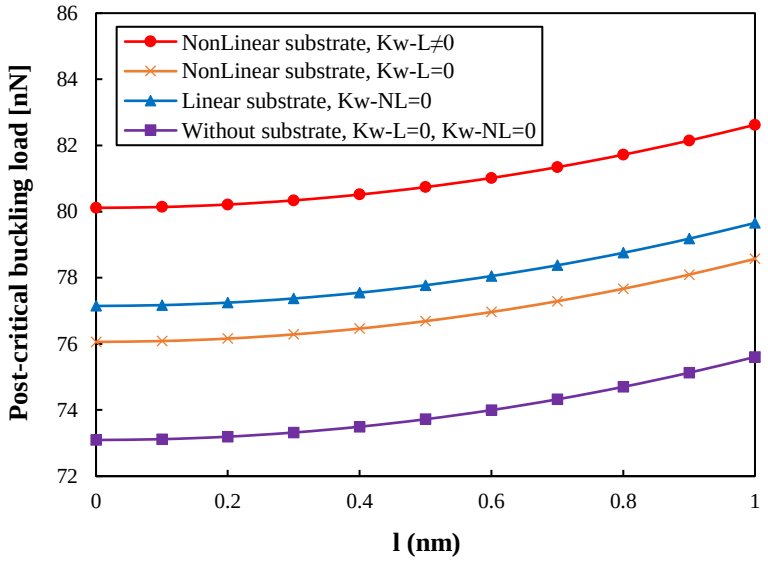

Fig. 6a. Effect of the linear Winkler medium vs. nonlinear one on the PCL (*L/d=20, θ=π/18, $k_{w\text{-}L}$=0.1GPa, $k_{w\text{-}NL}$=0.1GPa, e_0a=1 nm, SS*)

Figures 6b and 6c reveal a comparison between two terms of the Winkler foundation. This means it has linear behavior versus nonlinear one for different boundary conditions. For the first figure, the value of the nonlinear term is neglected and the second figure, the value of the linear term is chosen as 0.1GPa. From the first figure, it can be seen that an increase in the linear term of Winkler affects considerably CS boundary conditions. And

also, the results of these edges conditions tend to be closer to the SS boundary conditions. The galvanized result for clarifying the effect of the nonlinear term can be, however, the parallelism of the three curves in using the nonlinear term by Fig. 6c.

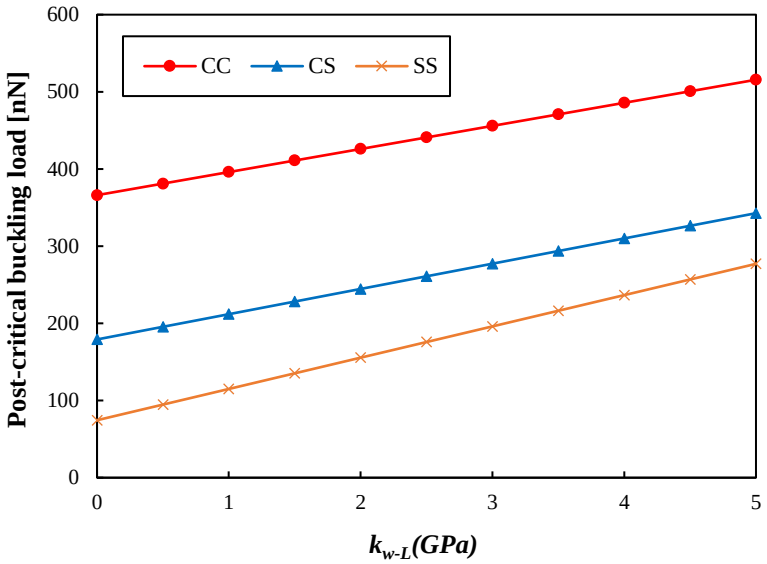

Fig. 6b. Effect of the Linear response of the foundation vs. various boundary conditions on the PCL (L/d=20, l=h, θ=$\pi/18$, e_0a=0.5 nm)

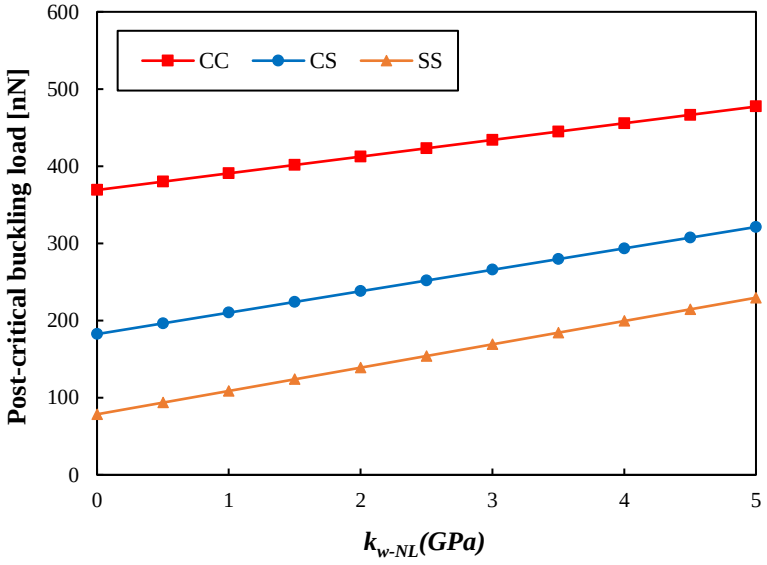

Fig. 6c. Effect of the nonlinear response of the foundation vs. various boundary conditions on the PCL (L/d=20, l=h, $k_{w\text{-}L}$=0.1GPa, θ=$\pi/18$, e_0a=0.5 nm)

Fig. 7a considers the effect of the taper angle for two boundary conditions, i.e. CC and CS groups in two cases of the matrix, linear and nonlinear behaviors. From this figure, one can observe that the nonlinear term of the foundation has no serious impact on the results of PCL under less flexible boundary conditions (clamped edges). In other words, in a CCNT with a large taper angle, there is no serious need to employ the nonlinear term of the matrix. Besides, it is seen that an increase in the taper angle generates the greater PCL which means that the taper angle establishes a stiffer nanotube.

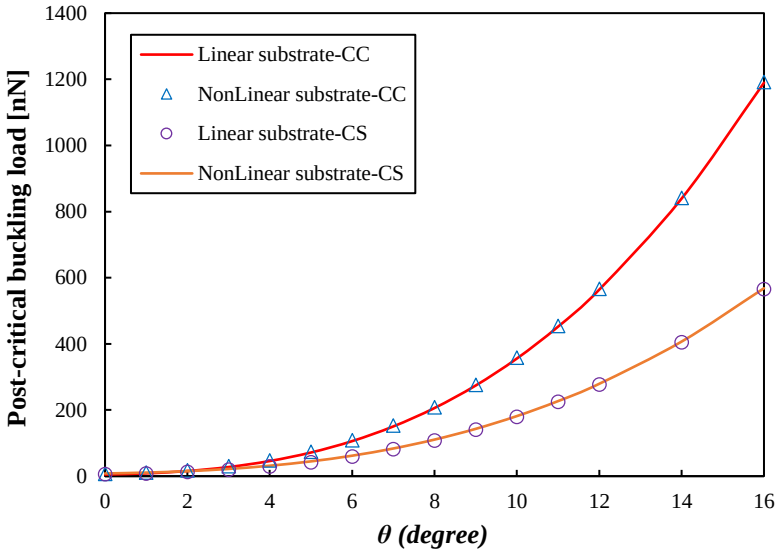

Fig. 7a. Effect of the taper angle vs. the Winkler foundation on the PCL (L/d=20, l=h, $k_{w\text{-}L}$=0.1GPa, $k_{w\text{-}NL}$=0.1GPa, e_0a=0.8 nm)

Fig. 7b shows the changes in the taper angle for CF and SS boundary conditions. It is germane to note that the increase of the taper angle leads to reducing the effect of the nonlinear term of the Winkler medium. This is due to the decline of the gap between the results of both nonlinear and linear foundation cases with increasing the conical angle. Furthermore, by comparing Fig. 7b with 7a, it is demonstrated that the influences of the

nonlinearity of the elastic matrix for nanotubes with CF and SS edge conditions are remarkably more than CC and CS ones. On the other hand, by looking at Fig. 7b, it is seen that the effect of the increase in the taper angle is noticeably more for the SS boundary conditions than CF ones. This is because the slope of the increase of the results of SS boundary conditions is considerably further than CF ones whilst the taper angle will increase. To conclude from Fig. 7a and Fig. 7b, one can claim that the effect of the nonlinear elastic foundation for less flexible boundary conditions is smaller.

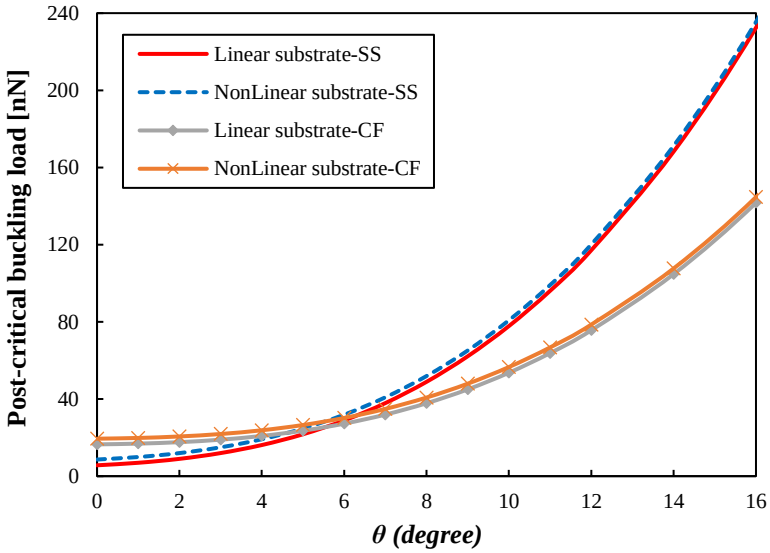

Fig. 7b. Effect of the taper angle vs. the Winkler foundation on the PCL (L/d=20, l=h, $k_{w\text{-}L}$=0.1GPa, $k_{w\text{-}NL}$=0.1GPa, e_0a=0.8 nm)

Fig. 7c depicts that by choosing the SS boundary conditions, the increase of the taper angle results in increasing the effect of surface in the CCNTs (because for SS when the surface effect is taken, at θ=0 and θ=10° the PCLs are 8.633 nN and 80.789 nN, respectively. But when the effect has been ignored, the post-buckling loads are 8.5593 nN and 78.7817 nN, respectively). This means that the gap of the numerical outcomes

(related to considering the surface effect and avoiding the effect) will be larger while the taper angle has been grown. This can be a rational conclusion in light of the increase of the taper angle which leads to an increase of the surface of the model and then the surface-to-volume ratio (STV). Therefore, more STV illustrates markedly the effect of the surface. As a matter of fact, for hinged boundaries, the surface effect is further significant than others. This can be proved by comparing the outcomes of SS boundary conditions and CF ones when the value of the taper angle has gone up. To conclude, although the results whilst the surface effect is investigated are approximately close to the results whilst the effect is neglected, the effect can play a crucial role in a small-scale domain in particular in some special situations and cannot be ignorable at all.

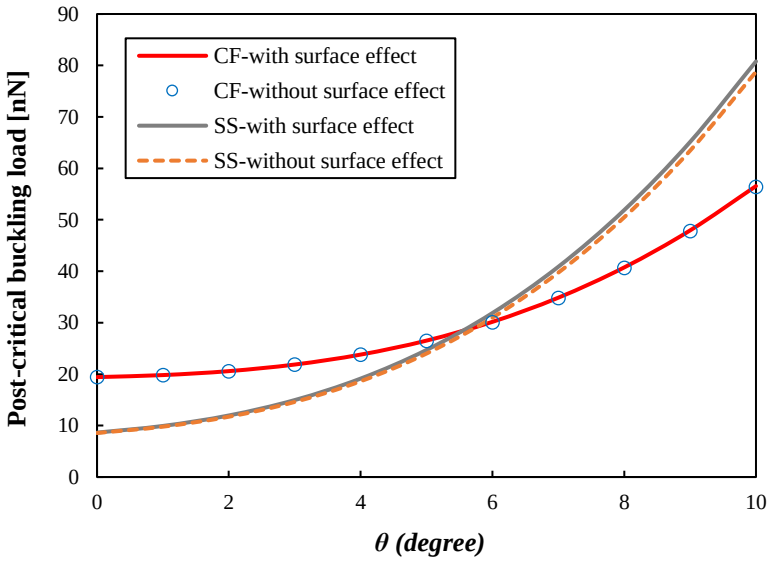

Fig. 7c. Effect of the taper angle vs. the surface effects on the PCL (L/d=20, l=h, $k_{w\text{-}L}$=0.1GPa, $k_{w\text{-}NL}$=0.1GPa, e_0a=0.8 nm)

Fig. 7d plots the results of the PCL for two boundary conditions, namely CF and SS with and without considering the Winkler base. This figure shows that whenever the

foundation has been removed, the numerical results for SS by the increase of the taper angle are more than CF at all. However, when the foundation is taken into consideration, before θ= 8, the results of SS are smaller than the CF. This behavior can be because of this fact that the elastic foundation makes the free edge of CCNT more rigid. Additionally, it can be found from this figure that by increasing the taper angle the importance of the foundation would be diminished. This is because of decreasing the distances of the curves between two cases; with the nonlinear foundation and without the substrate for both boundary conditions while the taper angle is getting larger.

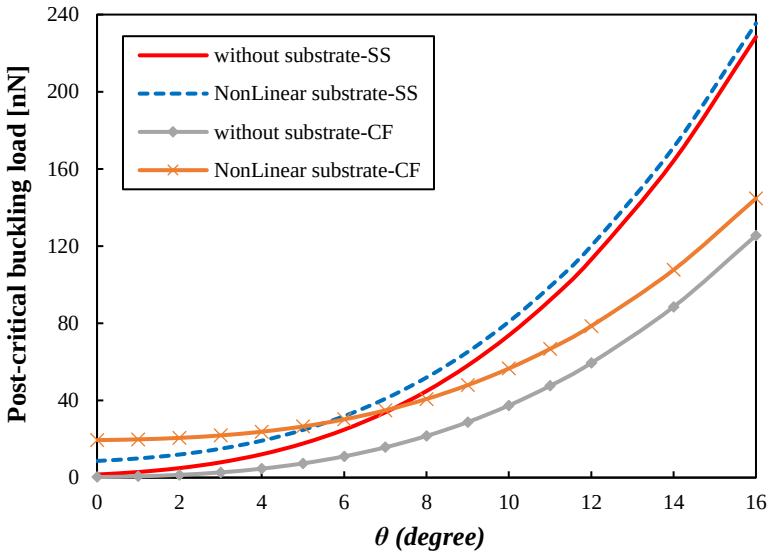

Fig. 7d. Effect of the taper angle vs. the Winkler foundation on the PCL (L/d=20, l=h, $k_{w\text{-}L}$=0.1GPa, $k_{w\text{-}NL}$=0.1GPa, e_0a=0.8 nm)

Fig. 8a and 8b exhibit the impact of nonlocality versus the surface effect along with different boundary conditions. As can be seen, with an increase in the nonlocal parameter the slope of reducing results for the less flexible boundary conditions is increased. Moreover, the increase of the nonlocality parameter does not affect the surface effect. In

addition, for CS and SS boundaries, the surface effect is a vital factor and for CC and CF ones the effect cannot play a serious role in order to analyze the nanostructure. It is interesting to declare that in CC boundary conditions, considering surface effect generates the results smaller than the manner of ignoring this effect. However, this behavior is completely reversed for SS, CF, and CS.

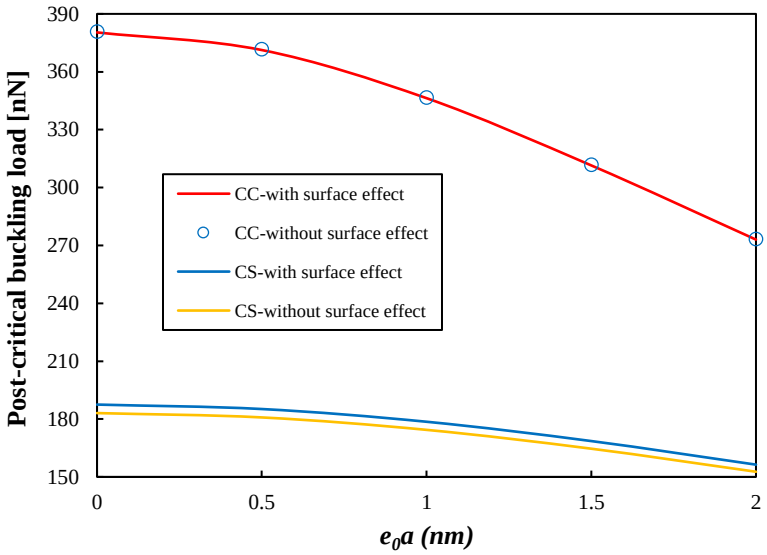

Fig. 8a. Effect of the nonlocal parameter vs. different boundary conditions on the PCL (L/d=20, $l=h$, $k_{w\text{-}L}=0.1GPa$, $k_{w\text{-}NL}=0.1GPa$, $\theta=\pi/18$)

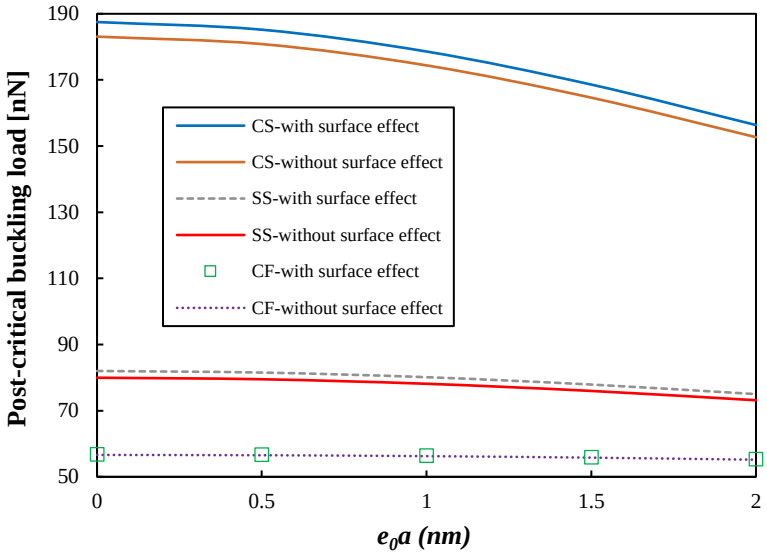

Fig. 8b. Effect of the nonlocal parameter vs. different boundary conditions on the PCL (L/d=20, $l=h$, $k_{w\text{-}L}=0.1GPa$, $k_{w\text{-}NL}=0.1GPa$, $\theta=\pi/18$)

5. Conclusions

This research was conducted to reveal the post-critical stability response of a truncated conical carbon nanotube by taking the nonlinear Winkler elastic substrate. To model the nanotube in the nanoscale domain, the surface, nonlocal and small size influences were captured. To solve the derived relations, the Rayleigh-Ritz semi-analytical solution technique was applied for which a new admissible function was also presented. The outcomes of this function perfectly showed its accuracy and precision. The numerical outcomes were demonstrated by figures and some obtained remark points are listed below:

* The CS and SS boundary conditions are influenced by the surface effect more than other ones.

* Increasing the taper angle increased the effect of surface and decreased the effect of the nonlinear term of the matrix.

* The taper angle increased remarkably the PCL for less flexible boundary conditions.

* The nonlinear term of the foundation was further effective for the more flexible boundary conditions.

* Taking the surface effect made the PCL larger for CF, CS and SS and smaller for CC boundary conditions.

Acknowledgements

The second author acknowledges the support of the Government of the Russian Federation (contract No. 14.Z50.31.0046).

References

[1] Z. Isfahani, M. T. Samadi, M. Alavi, N. Manuchehrpoor, M. Bakhani, Efficiency of Carbon Nanotubes in Municipal Solid Waste Landfill Leachate (Case Study: Treatment of Hamadan Landfill Leachate), Journal of water and Wastewater (in persian) 23 (2012) 67-72.

[2] S. Iijima, Helical microtubes of graphitic carbon, Nature 354 (1991) 56–8.

[3] S. Iijima, T. Ichihashi, Single-shell carbon nanotubes of 1-nm diameter, Nature 363 (1993) 603–635.

[4] W. J. Chang and S. S. Chu, Analytical solution of flexural vibration responses on taped atomic force microscope cantilevers, Physics Letters A 309 (2003) 133-137.

[5] W. J. Chang, T. H. Fang, H. L. Lee, and Y. C. Yang, Vibration sensitivity of the scanning near-field optical microscope with a tapered optical fiber probe, Ultramicroscopy 102 (2005) 85-92.

[6] I. C. Chen, L. H. Chen, X. R. Ye, C. Daraio, S. Jin, C. A. Orme, A. Quist, R. La, Extremely sharp carbon nanocone probes for atomic force microscopy imaging, Applied Physics Letters 88 (2006) 153102.

[7] K. Huo, X. Zhang, L. Hu, X. Sun, J. Fu, P. K. Chu, One-step growth and field emission properties of quasialigned Ti O_2 nanowire/carbon nanocone core-shell nanostructure arrays on Ti substrates, Applied Physics Letter 93 (2008) 013105.

[8] Z. Siwy, E. Heins, C. C. Harrell, P. Kohli, and C. R. Martin, Conical-nanotube ion-current rectifiers: the role of surface charge, Journal of the American Chemical Society 126 (2004) 10850-10851.

[9] L. T. Sexton, L. P. Horne, S. A. Sherrill, G. W. Bishop, L. A. Baker, and C. R. Martin, Resistive-Pulse Studies of Proteins and Protein/Antibody Complexes Using a Conical Nanotube Sensor, Journal of the American Chemical Society 129 (2007) 13144-13152.

[10] Zh. Lou, Ch. Chen, Q. Chen, Growth of Conical Carbon Nanotubes by Chemical Reduction of MgCO3, Journal of Physics and Chemistry B 109 (2005) 10557-10560.

[11] W. J. Chang, H. L. Lee, Free vibration of an embedded conical nanotube with surface effect, Digest Journal of Nanomaterials and Biostructures 8 (2013) 1325-1333.

[12] H. L. Lee, W. J. Chang, Surface effects on frequency analysis of nanotubes using nonlocal Timoshenko beam theory, Journal of Applied Physics 108 (2010) 093503.

[13] T. Chang, G. Li, X. Guo, Elastic axial buckling of carbon nanotubes via a molecular mechanics model, Carbon 43 (2005) 287–294.

[14] Y. Yan, W. Q. Wang, L. X. Zhang, Nonlocal effect on axially compressed buckling of triple-walled carbon nanotubes under temperature field, Applied Mathematical Modelling 34 (2010) 3422–3429.

[15] H. Shima, Buckling of Carbon Nanotubes: A State of the Art Review, Materials 5 (2012) 47-84.

[16] B. L. Wang, M. Hoffman, A. B. Yu, Buckling analysis of embedded nanotubes using gradient continuum theory, Mechanics of Materials 45 (2012) 52–60.

[17] H. M. Berrabah, N. Z. Sekrane and B. E. Adda, Buckling Analysis of Single-Walled Carbon Nanotubes Embedded in an Elastic Medium under Axial Compression Using Non-Local Timoshenko Beam Theory, Journal of Advanced Research in Applied Mechanics 17 (2016) 1-13.

[18] B. Akgöz, Ö. Civalek, A size-dependent beam model for stability of axially loaded carbon nanotubes surrounded by Pasternak elastic foundation, Composite Structures 176 (2017) 1028-1038.

[19] R. Rafiee, R. Maleki Moghadam, On the modeling of carbon nanotubes: A critical review, Composites Part B: Engineering 56 (2014) 435-449.

[20] L. J. Sudak, Column buckling of multiwalled carbon nanotubes using nonlocal continuum mechanics, Journal of Applied Physics 94 (2003) 7281.

[21] M. Rahmanian, M. A. Torkaman-Asadi, R. D. Firouz-Abadi, M. A. Kouchakzadeh, Free vibrations analysis of carbon nanotubes resting on Winkler foundations based on nonlocal models, Physica B: Condensed Matter 484 (2016) 83-94.

[22] R. Mao, F. H. Ling, Post-Critical Behavior of Thin-Walled Composite Beams, Thin-Walled Structures 18 (1994) 291-316.

[23] X. Song, S.-R. Li, Thermal buckling and post-buckling of pinned–fixed Euler–Bernoulli beams on an elastic foundation, Mechanics Research Communications 34 (2007) 164–171.

[24] N. Challamel, On the post-buckling of elastic beams on gradient foundation, C. R. Mecanique 339 (2011) 396–405.

[25] N. Silvestre, B. Faria, J. N. Canongia Lopes, A molecular dynamics study on the thickness and post-critical strength of carbon nanotubes, Composite Structures 94 (2012) 1352–1358.

[26] R. Ansari, R. Gholami, S. Sahmani, Prediction of compressive post-buckling behavior of single-walled carbon nanotubes in thermal environments, Applied Physics A 113 (2013) 145-153.

[27] S. D. Akbas, Large post-buckling behavior of Timoshenko beams under axial compression loads, Structural Engineering and Mechanics 51 (2014) 955-971.

[28] R. Ansari, M. Faghih Shojaei, V. Mohammadi, R. Gholami, H. Rouhi, Buckling and postbuckling of single-walled carbon nanotubes based on a nonlocal Timoshenko beam model, Journal of Applied Mathematics and Mechanics 95 (2014) 939-951.

[29] G.-L. She, F.-G. Yuan, Y.-R. Ren, W.-S. Xiao, On buckling and postbuckling behavior of nanotubes, International Journal of Engineering Science 121 (2017) 130–142.

[30] H. L. Dai , S. Ceballes , A. Abdelkefi , Y. Z. Hong , L. Wang , Exact modes for post-buckling characteristics of nonlocal nanobeams in a longitudinal magnetic field, Applied Mathematical Modelling 55 (2018) 758-775.

[31] H. Asadi, M. M. Aghdam, Large amplitude vibration and post-buckling analysis of variable cross-section composite beams on nonlinear elastic foundation, International Journal of Mechanical Sciences 79 (2014) 47–55.

[32] H. Babaei, Y. Kiani, M. R. Eslami, Thermal Buckling and Post-buckling Analysis of Geometrically Imperfect FGM Clamped Tubes on Nonlinear Elastic Foundation, Applied Mathematical Modelling 71 (2019) 12-30.

[33] C. W. Lim, G. Zhang, J. N. Reddy, A Higher-order nonlocal elasticity and strain gradient theory and Its Applications in wave propagation, Journal of the Mechanics and Physics of Solids 78 (2015) 298-313.

[34] G.-L. She, Y.-R. Ren, K.-M. Yan, On snap-buckling of porous FG curved nanobeams, Acta Astronautica 161 (2019) 475-484.

[35] G.-L. She, F.-G. Yuan, B. Karami, Y.-R. Ren, W.-S. Xiao, On nonlinear bending behavior of FG porous curved nanotubes, International Journal of Engineering Science 135 (2019) 58-74.

[36] M. R. Barati, N. M. Faleh, A. M. Zenkour, Dynamic response of nanobeams subjected to moving nanoparticles and hygro-thermal environments based on nonlocal strain gradient theory, Mechanics of Advanced Materials and Structures 26 (2019) 1661-1669.

[37] M. H. Ghayesh, A. Farajpour, Nonlinear coupled mechanics of nanotubes incorporating both nonlocal and strain gradient effects, Mechanics of Advanced Materials and Structures, (2018), https://doi.org/10.1080/15376494.2018.1473537.

[38] B. Karami, D. Shahsavari, M. Janghorban, Wave propagation analysis in functionally graded (FG) nanoplates under in-plane magnetic field based on nonlocal strain gradient theory and four variable refined plate theory, Mechanics of Advanced Materials and Structures 25 (2018) 1047-1057.

[39] M. Malikan, V. B. Nguyen, F. Tornabene, Damped forced vibration analysis of single-walled carbon nanotubes resting on viscoelastic foundation in thermal environment using nonlocal strain gradient theory, Engineering Science and Technology, an International Journal 21 (2018) 778-786.

[40] M. Malikan, V. B. Nguyen, Buckling analysis of piezo-magnetoelectric nanoplates in hygrothermal environment based on a novel one variable plate theory combining with higher-order nonlocal strain gradient theory, Physica E: Low-dimensional Systems and Nanostructures 102 (2018) 8-28.

[41] M. Malikan, R. Dimitri, F. Tornabene, Effect of sinusoidal corrugated geometries on the vibrational response of viscoelastic nanoplates, Applied Sciences 8 (2018) 1432.

[42] M. Malikan, V. B. Nguyen, F. Tornabene, Electromagnetic forced vibrations of composite nanoplates using nonlocal strain gradient theory, Materials Research Express 5 (2018) 075031.

[43] M. Malikan, R. Dimitri, F. Tornabene, Transient response of oscillated carbon nanotubes with an internal and external damping, Composites Part B: Engineering 158 (2019) 198-205.

[44] M. Malikan, V. B. Nguyen, R. Dimitri, F. Tornabene, Dynamic modeling of non-cylindrical curved viscoelastic single-walled carbon nanotubes based on the second gradient theory, Materials Research Express 6 (2019) 075041.

[45] S. K. Jena, S. Chakraverty, M. Malikan, Implementation of Haar wavelet, higher order Haar wavelet, and differential quadrature methods on buckling response of strain gradient nonlocal beam embedded in an elastic medium, Engineering with Computers (2019). https://doi.org/10.1007/s00366-019-00883-1

[46] S. K. Jena, S. Chakraverty, M. Malikan, F. Tornabene, Stability analysis of single-walled carbon nanotubes embedded in winkler foundation placed in a thermal environment considering the surface effect using a new refined beam theory (2019). https://doi.org/10.1080/15397734.2019.1698437

[47] M. Malikan, M. Krasheninnikov, V. A. Eremeyev, Torsional stability capacity of a nano-composite shell based on a nonlocal strain gradient shell model under a three-dimensional magnetic field, International Journal of Engineering Science (2020). https://doi.org/10.1016/j.ijengsci.2019.103210

[48] H. Abdoul-Anziz, P. Seppecher, C. Bellis, Homogenization of frame lattices leading to second gradient models coupling classical strain and strain-gradient terms, Mathematics and Mechanics of Solids 24 (2019) 3976-3999.

[49] R. Ansari, S. Sahmani, H. Rouhi, Axial buckling analysis of single-walled carbon nanotubes in thermal environments via the Rayleigh–Ritz technique, Computational Materials Science 50 (2011) 3050–3055.

[50] K. K. Pradhan, S. Chakraverty, Free vibration of Euler and Timoshenko functionally graded beams by Rayleigh–Ritz method, Composites: Part B 51 (2013) 175–184.

[51] M. Teifouet, A. Robinson, S. Adali, Buckling of nonuniform carbon nanotubes under concentrated and distributed axial loads, Mechanical Sciences 8 (2017) 299–305.

[52] M. Teifouet A. Robinson, S. Adali, Buckling of nonuniform and axially functionally graded nonlocal Timoshenko nanobeams on Winkler-Pasternak foundation, Composite Structures 206 (2018) 95-103.

[53] M. Malikan, M. Jabbarzadeh, S. Dastjerdi, Non-linear static stability of bi-layer carbon nanosheets resting on an elastic matrix under various types of in-plane shearing loads in thermo-elasticity using nonlocal continuum, Microsystem Technologies 23 (2017) 2973–2991.

[54] M. E. Golmakani, M. Malikan, M. N. Sadraee Far, H. R. Majidi, Bending and buckling formulation of graphene sheets based on nonlocal simple first order shear deformation theory, Materials Research Express 5 (2018) 065010.

[55] M. Malikan, M. N. Sadraee Far, Differential quadrature method for dynamic buckling of graphene sheet coupled by a viscoelastic medium using neperian frequency based on nonlocal elasticity theory, Journal of Applied and Computational Mechanics 4 (2018) 147-160.

[56] M. E. Golmakani, M. Ahmadpour, M. Malikan, Thermal buckling analysis of circular bilayer graphene sheets resting on an elastic matrix based on nonlocal continuum mechanics, Journal of Applied and Computational Mechanics (2019). DOI: 10.22055/JACM.2019.31299.1859

[57] X. J. Xu, X. C. Wang, M. L. Zheng, Z. Ma, Bending and buckling of nonlocal strain gradient elastic beams, Composite Structures 160 (2017) 366-377.

[58] X. J. Xu, Z. C. Deng, Variational principles for buckling and vibration of MWCNTs modeled by strain gradient theory, Applied Mathematics and Mechanics 35 (2014) 1115-28.

[59] M. T. A. Robinson, S. Adali, Variational solution for buckling of nonlocal carbon nanotubes under uniformly and triangularly distributed axial loads, Composite Structures 156 (2016) 101-107.

[60] M. H. Kahrobaiyan, M. Rahaeifard, M. T. Ahmadian, A nonlinear strain gradient beam formulation, International Journal of Engineering Science, 49 (2011) 1256-67.

[61] C. M. Wang, Y. Y. Zhang, S. S. Ramesh, S. Kitipornchai, Buckling analysis of micro- and nano-rods/tubes based on nonlocal Timoshenko beam theory, Journal of Physics D: Applied Physics 39 (2006) 3904-3909.

[62] S. C. Pradhan, G. K. Reddy, Buckling analysis of single walled carbon nanotube on Winkler foundation using nonlocal elasticity theory and DTM, Computational Materials Science 50 (2011) 1052–1056.

[63] J. B. Gunda, Thermal post-buckling & large amplitude free vibration analysis of Timoshenko beams: Simple closed-form solutions, Applied Mathematical Modelling 38 (2014) 4548–4558.

[64] R. Ansari, S. Sahmani, H. Rouhi, Rayleigh–Ritz axial buckling analysis of single-walled carbon nanotubes with different boundary conditions, Physics Letters A 375 (2011) 1255–1263.

[65] W. H. Duan, C. M. Wang, Exact solutions for axisymmetric bending of micro/nanoscale circular plates based on nonlocal plate theory, Nanotechnology 18 (2007) 385704.

[66] W. H. Duan, C. M. Wang, Y. Y. Zhang, Calibration of nonlocal scaling effect parameter for free vibration of carbon nanotubes by molecular dynamics, Journal of Applied Physics 101 (2007) 24305.

[67] A. C. Eringen, On differential equations of nonlocal elasticity and solutions of screw dislocation and surface waves, Journal of Applied Physics 54 (1983) 4703–4710.

[68] B. I. Yakobson, C. J. Brabec, J. Bernholc, Nanomechanics of carbon tubes: instabilities beyond linear response, Physical Review Letters 76 (1996) 2511–2514.

[69] R. E. Miller, V. B. Shenoy, Size-dependent elastic properties of nanosized structural elements, Nanotechnology 11 (2000) 139.

[70] X. Chen, C. Q. Fang, X. Wang, The influence of surface effect on vibration behaviors of carbon nanotubes under initial stress, Physica E 85 (2017) 47–55.

[71] J. Niiranen, V. Balobanov, J. Kiendl, S. B. Hosseini, Variational formulations, model comparisons and numerical methods for Euler–Bernoulli micro-and nano-beam models, Mathematics and Mechanics of Solids 24 (2019) 312-335.

[72] V. A. Eremeyev, On effective properties of materials at the nano-and microscales considering surface effects, Acta Mechanica 227 (2016) 29-42.

[73] P. S. Rao, S. Anandatheertha, G. Narayana Naik, S. Gopalakrishnan, Estimation of mechanical properties of single wall carbon nanotubes using molecular mechanics approach, Indian Academy of Sciences 40 (2015) 1301-1311.

[74] Y. Wang, X. Wang, X. Ni, H. Wu, Simulation of the elastic response and the buckling modes of single-walled carbon nanotubes, Computational Materials Science 32 (2005) 141-146.

[75] Y. J. Peng, L. Y. Zhang, Q. H. Jin, B. H. Li, D. T. Ding, Ab-initio studies of elastic properties and electronic structures of C and BN nanotubes, Physica E 33 (2006) 155-159.

[76] L. Li, Y. Hu, Post-buckling analysis of functionally graded nanobeams incorporating nonlocal stress and microstructure-dependent strain gradient effects, International Journal of Mechanical Sciences 120 (2017) 159-170.

[77] M. Meo, M. Rossi, A molecular-mechanics based finite element model for strength prediction of single wall carbon nanotubes, Materials Science and Engineering: A 454-455 (2007) 170-177.

[78] M. M. L. Treacy, T. W. Ebbesen, J. M. Gibson, Exceptionally high Young's modulus observed for individual carbon nanotubes, Nature (London) 381 (1996) 678–680.

[79] S. L. Mielke, D. Troy, S. Zhang, J. L. Li, S. Xiao, R. Car, R. S. Ruoff, G. C. Schatz, T. Belytschko, The role of vacancy defects and holes in the fracture of carbon nanotubes, Chemical Physics Letters 390 (2004) 413-420.

[80] Q. Ma, D. R. Clarke, Size Dependent Hardness in Silver Single Crystals, Journal of Materials Research 10 (1995) 853-863.

[81] W. J. Pooleh, M. F. Ashby, N. A. Fleck, Micro-Hardness of Annealed and Work-Hardened Copper Polycrystals, Scripta Materialia 34 (1996) 559-564.

[82] Y. Y. Lim, M. M. Chaudhri, Effect of the Indenter Load on the Nano hardness of Ductile Metals: An Experimental Study of Polycrystalline Work-Hardened and Annealed Oxygen-Free Copper, Philosophical Magazine A 79 (1999) 2979-3000.